remote sensing

MDPI

Article

Indian Land Carbon Sink Estimated from Surface and GOSAT Observations

Lorna Nayagam [1,*], Shamil Maksyutov [1], Rajesh Janardanan [1], Tomohiro Oda [2,3], Yogesh K. Tiwari [4], Gaddamidi Sreenivas [4], Amey Datye [4], Chaithanya D. Jain [5], Madineni Venkat Ratnam [5], Vinayak Sinha [6], Haseeb Hakkim [6], Yukio Terao [1], Manish Naja [7], Md. Kawser Ahmed [8], Hitoshi Mukai [1], Jiye Zeng [1], Johannes W. Kaiser [9], Yu Someya [1], Yukio Yoshida [1] and Tsuneo Matsunaga [1]

1 Earth System Division, National Institute for Environmental Studies, Tsukuba 305-8506, Japan; shamil@nies.go.jp (S.M.); rajesh.janardanan@nies.go.jp (R.J.)
2 Earth from Space Institute, Universities Space Research Association, Washington, DC 20024, USA
3 Department of Atmospheric and Oceanic Science, University of Maryland, College Park, MD 20742, USA
4 Indian Institute of Tropical Meteorology, Pune 411008, India
5 National Atmospheric Research Laboratory, Gadanki 517112, India
6 Indian Institute of Science Education and Research, Mohali 140306, India
7 Aryabhatta Research Institute of Observational Sciences, Nainital 263001, India
8 Department of Oceanography, Faculty of Earth and Environmental Sciences, University of Dhaka, Dhaka 1000, Bangladesh
9 The Climate and Environmental Research Institute NILU, 2027, Kjeller, Norway
* Correspondence: raja.nayagam.lorna@nies.go.jp

Abstract: The carbon sink over land plays a key role in the mitigation of climate change by removing carbon dioxide (CO_2) from the atmosphere. Accurately assessing the land sink capacity across regions should contribute to better future climate projections and help guide the mitigation of global emissions towards the Paris Agreement. This study estimates terrestrial CO_2 fluxes over India using a high-resolution global inverse model that assimilates surface observations from the global observation network and the Indian subcontinent, airborne sampling from Brazil, and data from the Greenhouse gas Observing SATellite (GOSAT) satellite. The inverse model optimizes terrestrial biosphere fluxes and ocean-atmosphere CO_2 exchanges independently, and it obtains CO_2 fluxes over large land and ocean regions that are comparable to a multi-model estimate from a previous model intercomparison study. The sensitivity of optimized fluxes to the weights of the GOSAT satellite data and regional surface station data in the inverse calculations is also examined. It was found that the carbon sink over the South Asian region is reduced when the weight of the GOSAT data is reduced along with a stricter data filtering. Over India, our result shows a carbon sink of 0.040 ± 0.133 PgC yr^{-1} using both GOSAT and global surface data, while the sink increases to 0.147 ± 0.094 PgC yr^{-1} by adding data from the Indian subcontinent. This demonstrates that surface observations from the Indian subcontinent provide a significant additional constraint on the flux estimates, suggesting an increased sink over the region. Thus, this study highlights the importance of Indian subcontinental measurements in estimating the terrestrial CO_2 fluxes over India. Additionally, the findings suggest that obtaining robust estimates solely using the GOSAT satellite data could be challenging since the GOSAT satellite data yield significantly varies over seasons, particularly with increased rain and cloud frequency.

Keywords: carbon dioxide; Indian CO_2 flux; South Asian biosphere; GOSAT; OCO-2 MIP; CO_2 fluxes; carbon sink

Academic Editor: Bassil El Masri

Received: 6 November 2024
Revised: 15 January 2025
Accepted: 18 January 2025
Published: 28 January 2025

Citation: Nayagam, L.; Maksyutov, S.; Janardanan, R.; Oda, T.; Tiwari, Y.K.; Sreenivas, G.; Datye, A.; Jain, C.D.; Ratnam, M.V.; Sinha, V.; et al. Indian Land Carbon Sink Estimated from Surface and GOSAT Observations. *Remote Sens.* **2025**, *17*, 450. https://doi.org/10.3390/rs17030450

1. Introduction

The increase in carbon dioxide (CO_2) emissions is the primary cause of global warming. Recent reports indicate that CO_2 emissions from developing nations are rising [1]. Factors such as population growth, land use changes, urbanization and industrialization have led South Asian countries, such as India, Pakistan, Bangladesh, Nepal, Bhutan, and Sri Lanka, to make notable contributions toward global emissions [2]. This increase in emissions has diminished the carbon sink capacity of the region, which has seen a decline in carbon sink from -0.49 to -0.37 ± 0.20 PgC yr^{-1} [3,4], approaching a near-neutral state [5]. Since India accounts for a large fraction (72%) of the South Asian landmass, assessing the land biosphere over the region is important in obtaining an overall understanding of the carbon cycle.

Top-down methods are commonly used to obtain estimates of terrestrial CO_2 fluxes using atmospheric CO_2 measurement data (e.g., [6]). Initially, these efforts focused on quantifying fluxes over large land regions, such as the TRANSCOM-3 regions [7,8]. A study on Asian fluxes was presented in [9], which focused on understanding the fluxes of the Eurasian Temperate region by assimilating CO_2 observations from several ground sites in Asia and Sydney–Tokyo passenger aircrafts in a global inverse model. Subsequent research concentrated on estimating regional fluxes by combining datasets from different platforms [10,11]. Thus, the South Asian fluxes were also estimated using Civil Aircraft for the Regular Investigation of the Atmosphere Based on an Instrument Container (CARIBIC), Comprehensive Observation Network for Trace gases by Airliner (CONTRAIL), and surface datasets [3,4,12,13], with a special focus on the Indian subcontinent. However, the lack of sufficient observations, particularly in certain key regions, such as South Asia and Africa, poses a challenge in obtaining robust emission estimates [14], leaving the estimates highly uncertain over such data-sparse regions. This challenge is more critical for obtaining top-down fluxes at a policy-relevant scale, as attempted by [15,16]. Over the past decade, space carbon observing missions, such as GOSAT, GOSAT-2, and OCO-2/3, have attempted to overcome this data challenge and achieve the robust estimation of terrestrial CO_2 fluxes [16,17]. Similar attempts have also been conducted to determine Indian CO_2 emissions using both in situ and satellite data [5,18–21].

Despite efforts to obtain robust top-down flux estimates, the terrestrial biospheric CO_2 fluxes obtained using bottom-up and top-down approaches have shown large discrepancies [16,22]. Over India, the biospheric flux estimated using the top-down approach varies between -0.27 and -0.08 PgC yr^{-1} [21], whereas it is as high as -0.38 PgC yr^{-1} to -0.53 PgC yr^{-1} [23] using a bottom-up approach, which highlights the potential weak understanding of the net carbon budget in the area. Moreover, CO_2 emissions are also influenced by large-to-regional scale climate phenomena, such as monsoons and the El Niño. Thus, knowledge of the variability in the CO_2 concentration and the exchange of terrestrial biospheric fluxes over the region is significant [24–29].

In this study, we calculate the terrestrial biospheric CO_2 fluxes over India using a high-resolution global flux inverse model (NIES-TM-Flexpart-VAR, [30]) to assess its contribution towards the total emissions over the South Asian region. We utilize various atmospheric measurement data available in the region for 2016–2023, such as surface site data from the global reference network (ObsPack, [31,32], a regional Indian subcontinent surface network (out of the three inland sites, each one is maintained by the Indian Institute of Tropical Meteorology (IITM), the Indian Institute of Science Education and Research (IISER) and the National Atmospheric Research Laboratory (NARL), India, and two other sites are maintained by the National Institute for Environmental Studies (NIES), Japan), and additional regional observations by NIES, aircraft vertical profile data from Brazil, and Greenhouse gases Observing Satellite (GOSAT) data in order to obtain biospheric CO_2

flux estimates across the globe. Previous studies estimated the biospheric CO_2 emissions over India either by utilizing satellite data (XCO_2) or limited surface CO_2 datasets. Hence, estimates based on datasets from different platforms, such as both surface and satellites, are lacking. In comparison to past studies, we use data with a wider surface coverage over India and rely on a higher-resolution transport model. Including more observations in the inversion helps the model to optimize the fluxes better by allowing the model to give corrections in regions with notable CO_2 variability and avoid producing irrelevant adjustments. Therefore, this study focuses on the impact of additional surface measurement data from the Indian subcontinent network on the South Asian and Indian land CO_2 fluxes. The results are evaluated with independent measurements from the Sinhagad (SNG) site near Pune, India. As the observations from other Indian sites are used in the inversions, only SNG is used for validation. We also examine the sensitivity of the inverse model estimation to the uncertainty assigned to the GOSAT data and the effect of Comilla (CLA) measurements in the inversions.

2. CO_2 Data

2.1. Surface Measurements

2.1.1. ObsPack Datasets

We use two versions of the ObsPack [31,32], which include surface measurements across the globe. Version 9.0 of the ObsPack (ObsPack_co2_1_GLOBALVIEWplus_v9.0) provides the dry air CO_2 mole fraction for the period 2009–2022, and version 9.2 of the ObsPack (ObsPack_co2_1_NRT_v9.2) provides data for 2023 to 2024. Our data selection criteria (observation sites for data assimilation and times of the day) are based on the approach used by the OCO-2 MIP project [15], with some additional observation sites (See Table S1). The selection procedure checks the assimilate flag in the ObsPack flask data, while for continuous sites, the selection follows the OCO-2 MIP list, extended by adding continuous observation sites with data records available for more than 5 years over the East Asia and Europe regions. Aircraft observations were not included in the data assimilation. For the tower sites with multiple vertical data levels, the topmost data level was selected. As a result, in the 2016–2023 period, data from 158 ObsPack data records were assimilated. The data uncertainty assigned to each site was set based on the mode observation fit (mean Root Mean Square Error (RMSE)) using the surface-optimized forward simulations that we prepared for the OCO-2 MIP project [15], with the minimum value set to 0.5 ppm. The data were not used for data assimilation if the prior residuals were three times (or more) larger than the data uncertainty. Sites with a mean RMSE of more than 5 ppm were also omitted. Table S1 in the Supplementary Material details all the surface/aircraft sites used in this study.

2.1.2. Measurements from the Surface Network in India and Nearby Region

The surface CO_2 dry air mole fraction from the five Indian site, namely Gadanki (GAD), Mohali (MOH), Nainital (NTL), Pune (PUN), Sinhagad (SNG) (see details in Table 1) and Comilla (CLA) (Bangladesh) (hereafter Indian sub-continental measurements), are included in this study. The measurements for the sites NTL and CLA are weekly flask data from NIES. NTL is a mountain site situated near the Himalayas [33,34]. The site is considered to be less influenced by anthropogenic emissions. Hence, NTL is considered a background site for India, whereas CLA [33] is located on the Indo-Gangetic Plain (IGP). However, the site may be influenced by local CO_2 emissions from anthropogenic activities and biomass burning in the region. Monsoon winds play a significant role in modulating the emissions of the region [35]. MOH is a suburban site [36] near the city of Chandigarh and is also situated in IGP; in addition, PUN is a suburban site [37] located near the city of Pune. As MOH

and PUN are situated near cities, the sites are influenced by the higher fossil fuel activities in the surroundings; meanwhile, GAD is a rural site [24], influenced by the atmospheric circulation during monsoon seasons in India. Thus, the CO_2 emissions from local biomass burning and agricultural activities are carried to this site. Except for NTL, the sites used in the Indian network are influenced by the CO_2 emissions from anthropogenic activities. These sites are well distributed across the country to suitably represent the emissions from south to north and from west to east (including CLA). Hence, these observations are significant in the estimation of emissions and sinks over the region.

Table 1. Details of CO_2 measuring sites from the Indian network and Comilla, Bangladesh. $^+$ used for validation.

Site Code	Station	Latitude	Longitude	Elevation (m)	Sampling Height (m)	Data Source	Sampling
CLA	Comilla	23.43	91.18	30	8	NIES	Flask
GAD	Gadanki	13.5	79.18	350	10	NARL	in-situ
MOH	Mohali	30.67	76.73	310	20	IISER	in-situ
NTL	Nainital	29.36	79.46	1940	7	NIES	Flask
PUN	Pune	18.54	73.81	520	-	IITM	in-situ
SNG$^+$	Sinhagad	18.37	73.75	1311	-	IITM	in-situ

2.1.3. Auxiliary Observations

The surface CO_2 observations collected by NIES over the three sites in Japan (Cape Ochi-ishi, Hateruma Island [38,39] and Mount Fuji [40]) are included in this study. These observations provide an additional constraint for the model, allowing a better estimation of the land fluxes in South Asia. Furthermore, airborne measurements taken below a 1 km altitude from three sites in Brazil (ALT, SAN, TEF) [41,42] were also included to enhance the background information, which is otherwise limited by the few data points over South America.

2.2. GOSAT Satellite Observations

Besides surface measurements, column CO_2 observations from the GOSAT satellite are also used to constrain the inverse model. GOSAT is the first satellite to measure GHG gases from space using the onboard Thermal and Near Infrared Sensor for Carbon Observation—Fourier Transform Spectrometer (TANSO-FTS) instrument [43,44]. Satellite data are taken from the bias-corrected column average concentration retrievals in the NIES Level 2 XCO_2 product v03.05 [45,46], subsetted for the "general user". In addition to the bias correction already applied to the XCO_2 product, the data are corrected by subtracting the monthly mean biases for each 5° latitude band of the retrieved XCO_2 against forward simulations using fluxes optimized with ObsPack data inversion. The bias is calculated separately for three GOSAT observation modes: land nadir, ocean glint, and land medium gain (most data are taken in a high gain mode). The XCO_2 simulation performed by the transport model takes into account the vertically varying contribution to XCO_2 of the simulated CO_2 profile expressed by the column-averaging kernel from the retrieval product, as recommended in [47].

2.3. Independent Measurements for Validation

Sinhagad (SNG) is a near semi-urban mountain site at 1311 m above sea level, making continuous observations, operated by the Indian Institute of Tropical Meteorology (IITM), Pune, Ministry of Earth Sciences, Government of India [48]. It helps to monitor the CO_2 levels over the region. Though the frequent and well-calibrated measurements are promis-

ing for its use in inversion, the data record is limited to 2023 and hence is used only for independent validation. Other sites are already included in inversion or located in areas impacted by local fluxes, and are thus less suitable for validation. Figure 1 shows the location of the site.

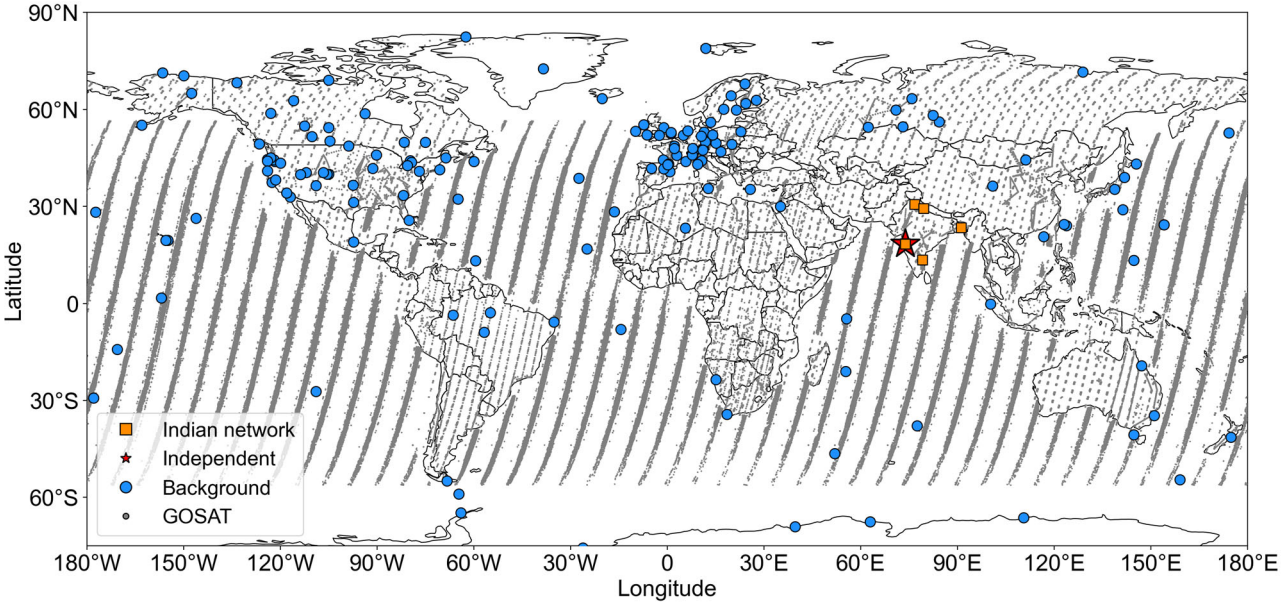

Figure 1. The locations of the Indian observation sites (orange squares), global surface observations from ObsPack (blue dots), and GOSAT (grey dots) observations. The data site SNG, used for independent validation, is also shown (red star).

3. Prior Fluxes

The prior fluxes used in this study include the monthly varying ocean–atmosphere exchange estimated with a neural network model [49,50]; the emissions caused by biomass, derived from the Global Fire Assimilation System (GFASv1.2 [51]) using Fire Radiative Power (FRP) measurements obtained from the Moderate Resolution Imaging Spectroradiometer (MODIS); and the ten-day mean of emissions and uptake by vegetation (all but ocean are at a 0.1° resolution). This includes gross primary production (GPP) and ecosystem respiration (RECO), which are determined by combining remote sensing data and tower fluxes with machine learning [52,53]. Fossil fuel emissions are provided by a combination of ODIAC v2020 [54] land data remapped from a 1 km to 0.1° resolution with ship-borne emissions by EDGAR v.6.0, while the monthly global totals are adjusted to match the data obtained by Basu and Nassar (2021) [55]. ODIAC data after 2019 are taken from ODIAC v2022 [54]. Ocean fluxes are interpolated to a 0.1° resolution and adjusted with a high-resolution land mask. After 2019, land vegetation and ocean fluxes are set to the same as those for the last available year. Links to the datasets are provided in the data availability section.

Prior Uncertainties

The prior flux uncertainty fields were prepared at a 0.1° × 0.1° resolution for the fluxes optimized by the model. The uncertainty for the terrestrial vegetation net ecosystem exchange is based on climatological mean monthly respiration flux data and is distributed geographically and seasonally in accordance with remote sensing data regarding productivity and temperature; thus, they provide a better spatially varying guess for the uncertainty of the net ecosystem exchange fluxes. Therefore, the respiration fluxes have wider seasonal coverage than GPP and can be used to adjust fluxes in a dormant season. Similarly, the

ocean–atmosphere exchange is prepared by interpolating the 1° × 1° ocean flux uncertainty dataset, as in [30]. The interpolated fluxes were set to zero over land using land area fraction data derived from 1 km resolution MODIS vegetation cover data. The biomass burning fluxes are not optimized and not accounted for in the uncertainty, assuming that the ecosystem respiration-based spatial uncertainty pattern provides the necessary degree of freedom for adjusting the net CO_2 flux at a large scale.

4. Inverse Modeling Technique

This study utilizes the NIES-TM-FLEXPART-variational (NTFVAR), a Lagrangian–Eulerian coupled model, to optimize the biospheric and oceanic fluxes. The model uses the flux datasets to calculate the simulated concentration, employing the same surface fluxes in the Lagrangian and Eulerian component models [30,56]. The contribution of surface fluxes to the observed concentration for the last three days is calculated by the high-resolution Lagrangian model FLEXPART v.8.0, which also uses the 3D CO_2 concentrations simulated on a 3.75° × 3.75° 42-level grid via the Eulerian model NIES-TM v.20 as initial and boundary conditions. As in [57], we use hourly ERA5 reanalysis data on the model grid to prepare average mass fluxes on a 42-level hybrid-pressure grid for NIES-TM. FLEXPART surface flux footprints are calculated with JRA-55 reanalysis data separately for daytime and nighttime fluxes, for use with the diurnally varying biospheric fluxes provided by 10 daily datasets of ecosystem respiration and gross primary production (representing daytime uptake), as in [53]. The daily mean respiration and GPP are expanded flatly into hourly fluxes, the respiration for the whole day, and the GPP for daytime only. To reduce internal memory use, the inverse-model-optimized flux corrections are prepared as a multiple of two spatially varying functions: the flux uncertainty field and scaling factor. The scaling factor is prepared at 0.2° × 0.2°, while the flux uncertainty is provided at a 0.1° × 0.1° resolution. Following [57], the NTFVAR model applies a spatial flux covariance length of 50 km, which is suitable for studying the regional gradients in the land fluxes.

Experiment Setup

The inversions are carried out by incorporating surface (global and regional) and GOSAT satellite measurements to estimate biospheric CO_2 fluxes from the inverse model. Two sets of inversions were performed: (i) inversions that assimilate measurements from the Indian subcontinent (ISG, ISGH, and I4SG) and (ii) inversions that do not include these measurements (SG, SGH). All these inversions use global surface and GOSAT observations; however, the weights assigned to the GOSAT measurements differ. In addition, the number of sites from the Indian subcontinent also varies. Thus, the inversions ISG and ISGH include data from five sites in the Indian subcontinent (I), the global surface (S), and GOSAT (G) measurements; however, the uncertainty of the GOSAT measurements is moderate or high (H), respectively. However, in I4SG, the CLA site is excluded, while data from the other four sites within the Indian network (I4) are retained. This allows us to comprehend the significant variability found in the measurements from the CLA site and its impact on Indian biospheric flux estimates. Additionally, a corresponding set of inversions assimilating the observations from the global surface and GOSAT satellite (SG and SGH) is carried out. This set of inversions does not include Indian subcontinental measurements. Table 2 provides detailed information about the inversions.

The corrections for the land biosphere and ocean–atmosphere fluxes were obtained by supplying the uncertainty files corresponding to these fluxes, along with the priors. The estimates of Indian biospheric CO_2 fluxes include correction for the lateral carbon transport through riverine outflow and crop/wood trading, as indicated in previous

studies [58,59]. The estimates for South Asia/India are the mean of the multiyear annual totals for 2016–2023 and the uncertainty is its standard deviation.

Table 2. The details of the different sets of inversions carried out in the study.

Inversions	5 Sites from Indian Subcontinent			GOSAT		Global Surface
	Indian Network (4 Sites)	Site CLA				
		Uncertainty (ppm)	Rejection	Uncertainty (ppm)	Rejection	
ISG	Yes	9	1 s	8	1 s	Yes
ISGH	Yes	9	1 s	16	0.5 s	Yes
I4SG	Yes	No		8	1 s	Yes
SG	No	No		8	1 s	Yes
SGH	No	No		16	0.5 s	Yes

5. Results

5.1. Optimized Mean Annual Biospheric CO_2 Flux and Selected OCO-2 MIP Models

The inversions ISG, ISGH, and I4SG (without CLA) are carried out by including all the observations mentioned in the data section. The ability of our inversions to represent the regional land fluxes was analyzed and compared to the fluxes from a subset of OCO-2 MIP models. The global total fluxes from our inversions were −4.36, −4.45, and −4.37 PgC yr^{-1} for ISG, ISGH, and I4SG, respectively. The South Asian fluxes calculated from our inversions (−0.23 to −0.18 PgC yr^{-1}) fall within the multi-model spread of OCO-2 MIP models (−0.35 to 0.2 PgC yr^{-1}); hence, the estimated fluxes are considered to be in a reasonable range. The aggregated fluxes for the South Asian region from this study and selected OCO-2 MIP models are given in Figure 2. The outputs from Carbon Tracker (CT), Transport Model 5—Four-Dimensional Variational model (TM5-4DVAR), Copernicus Atmosphere Monitoring Service (CAMS), OU (TM5-based model) and Baker (PCTM based model) are the simulation names used in [15].

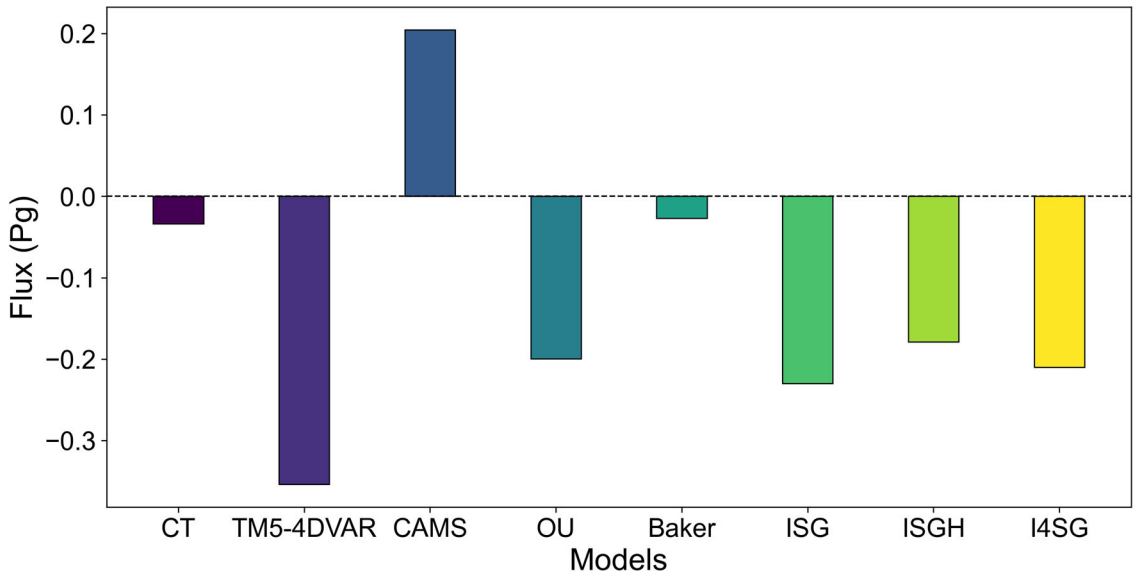

Figure 2. The South Asian flux estimates obtained by a subset of the OCO-2 MIP models (see [15] for individual model details) and our model. CT, TM5-4DVAR, CAMS, OU, and Baker are the selected OCO-2 MIP models. ISG, ISGH, and I4SG represent the different inversions carried out with the NTFVAR model.

The seasonal variation at selected global background sites was also examined (Figure 3). The optimized concentrations follow the observed measurements, which confirms the ability of our model to reproduce the seasonal cycle at these sites well. As the inversions realistically represent the sinks and sources of the global land regions and represent the seasonal cycle at global background sites, we focus on the fluxes over South Asia to comprehend the improvement in inversions with the addition of Indian sub-continental observations.

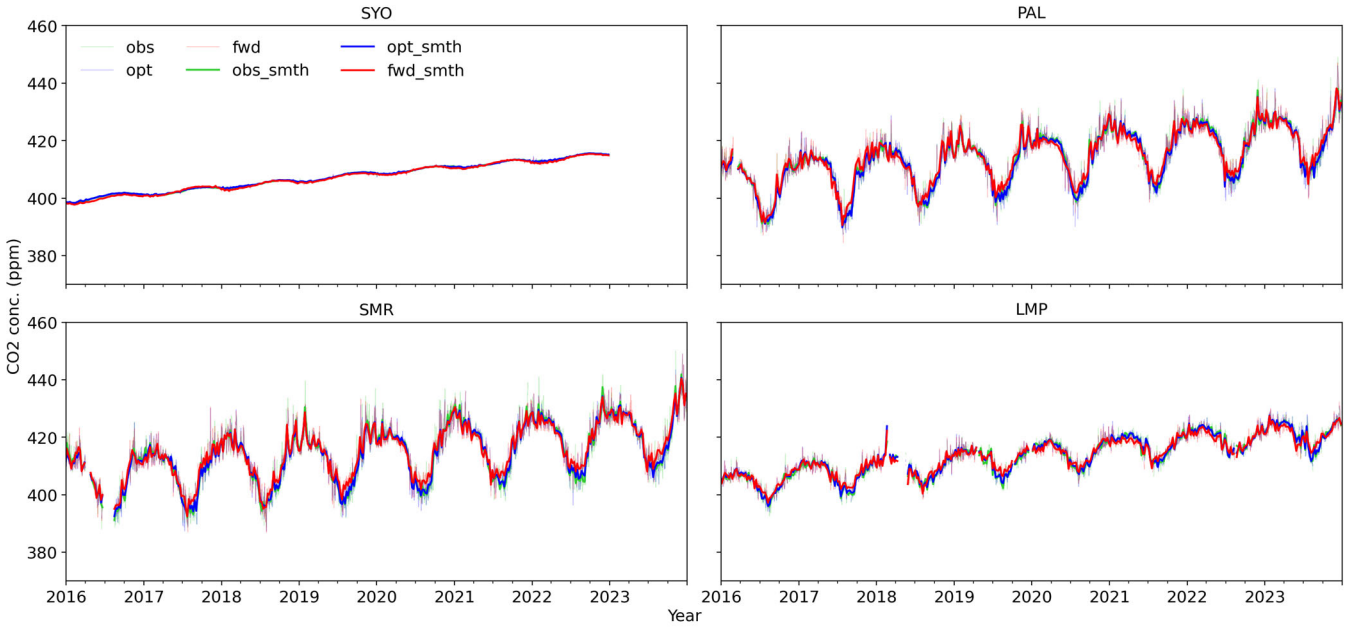

Figure 3. Time series of observation (green), forward (red), and optimized (blue) simulations for the selected background sites Syowa (SYO), Pallas (PAL), Hyytiälä (SMR) and Lampedusa (LMP). The smoothed values are the weekly averages of daily measures.

5.2. Assessment of South Asian Land Fluxes

The South Asian region has a greater significance in global inversions, as the flux estimates of this region are highly uncertain due to the uncertainties in the bottom-up inventories and lack of adequate surface-based observations. Hence, the ability of the Indian sub-continental observations to aid in estimating the South Asian fluxes is analyzed by including/not including those measurements in the inversions; however, the lateral transport is not considered here.

5.2.1. Inversions with Indian Sub-Continental Measurements

The regional biospheric fluxes obtained from inversions ISG, ISGH, and I4SG are -0.23, 0.18, and 0.21 PgC yr^{-1}, respectively; this implies that the South Asian sink obtained from ISG is stronger compared to the carbon sink obtained from ISGH and I4SG. In ISG, GOSAT measurements have a moderate uncertainty (8 ppm), whereas, in ISGH, it is double (16 ppm, but with stricter filtering) that in ISG. Therefore, the South Asian fluxes from ISG and ISGH were different. However, in these two inversions, the uncertainty of CLA measurements remained the same (9 ppm). The CO_2 fluxes obtained from ISG (with CLA) and I4SG (without CLA) with the same weights of the GOSAT measurements (uncertainty 8ppm and sigma 1) were similar (-0.23 and -0.21 PgC yr^{-1}, respectively). Thus, the presence or absence of CLA measurements in the inversions does not have a larger influence on the South Asian fluxes; yet, the uncertainty of GOSAT measurements has a considerable impact on the South Asian fluxes.

5.2.2. Inversions Without Indian Sub-Continental Measurements

Another set of inversions was also conducted, namely SG and SGH. Here, the model parameters remain the same as in the previous set, but inversions are carried out without the Indian sub-continental measurements. For SG, the South Asian sink is weaker (-0.12 PgC yr^{-1}) than that for ISG (with Indian sub-continental measurements), whereas a near-neutral sink (-0.04 PgC yr^{-1}) is obtained for SGH, where the uncertainties for GOSAT measurements (with stricter filtering) are higher than those for SG. Thus, the absence of Indian sub-continental measurements leads to a reduction in the South Asian fluxes in the two inversions, namely SG and SGH. The result from our inversions is comparable to the results from [5], which uses global surface and OCO-2 measurements to estimate the biospheric fluxes over South Asia to obtain a near-neutral value of -0.04 ± 0.14 PgC yr^{-1}.

In short, including Indian sub-continental measurements along with global surface sites and GOSAT (with moderate uncertainty) during inversion (ISG) led to an increase in the South Asian sink. However, the South Asian sink was reduced in ISGH, as the GOSAT measurements had higher uncertainty (but stricter filtering). However, without Indian sub-continental measurements in the inversions, the South Asian sink was reduced for both SG and SGH, with a stronger sink for SG compared to SGH.

5.3. Assessment of Land Biospheric Fluxes over India

We further evaluate the fluxes over India using the inversions; however, their fluxes differ over the South Asian region.

5.3.1. Inversions with Indian Sub-Continental Measurements (ISG, ISGH, and I4SG)

The land flux over India is calculated and compared to the inventory reports for UNFCCC compiled by [60]. The average flux over India for the period 2016–2023 from the ISG is -0.223 PgC yr^{-1}. We consider the lateral carbon transport by crop and wood trade and rivers [61], and obtain an adjusted value of -0.147 ± 0.09 PgC yr^{-1} for comparison with land carbon stock changes. Similarly, for ISGH and I4SG, the adjusted fluxes are -0.096 ± 0.08 and -0.131 ± 0.1 PgC yr^{-1}, respectively. The model is constrained by the supplied observation to give an increased sink over India (ISG, I4SG; moderate GOSAT uncertainty), but the sink decreases in ISGH. The sink is slightly reduced in I4SG too, due to the absence of CLA measurements in the inversions. Our estimates (-0.096–-0.147 PgC yr^{-1}) are slightly higher than the median value of -0.065 ± 0.02 PgC yr^{-1}, obtained from an ensemble of models using in situ global surface measurements [60]; however, they are comparable to the results (-0.08 to -0.27 PgC yr^{-1}) obtained in [21] when using the Indian surface CO_2 measurements and the bottom-up estimate of [62] (-0.16 ± 0.02 PgC yr^{-1}).

5.3.2. Inversions Without Indian Sub-Continental Measurements (SG and SGH)

The biospheric flux calculated from the inversions when not including the Indian sub-continental measurements generally saw a reduction in the CO_2 flux. From the SG inversion, the terrestrial flux obtained is -0.116 ± 0.133 PgC yr^{-1}, and after adjusting for lateral transport, the flux is -0.040 ± 0.133 PgC yr^{-1} over the country. The CO_2 flux over India from the SGH case is -0.048 ± 0.045 PgC yr^{-1}, and the adjusted value is 0.028 ± 0.046 PgC yr^{-1}, indicating a weak source. The reduction in the uncertainty of fluxes in the SGH case could be due to the stricter filtering of GOSAT measurements. The top-down and bottom-up estimates for India from recent studies are given in Table 3.

Table 3. Top-down/bottom-up estimates of Indian biospheric CO_2 fluxes from recent studies (* lateral carbon transport included, # estimate over temperate Eurasia).

Top-Down Estimates					
Recent Studies	**Model Used**	**CO_2 Observation**	**Indian CO_2 Observation**	**Period of Study**	**Fluxes PgC yr^{-1}**
Swathi et al.,2021 [21]	LMDZ	Insitu (global)	3 sites	2006–2011	−0.27 to −0.08
Halder et al., 2022 [18]	NIES-TM	Insitu (global) + GOSAT	2 sites	2010–2012	0.33 ± 0.57 #
Deng et al., 2024 [60]	Ensemble	Insitu (global)	CONTRAIL	2015–2019	−0.065 ± 0.02 *
Deng et al., 2024 [60]	Ensemble	GOSAT/ OCO-2	Satellite only	2015–2021	−0.065 ± 0.06 *
This study	NTFVAR	Insitu (global) + GOSAT + CLA (Bangladesh)	4 sites	2016–2023	−0.147 ± 0.09 *
Bottom-Up Estimates					
Study		**Data Used**		**Period of Study**	**Fluxes PgC yr^{-1}**
Nayak et al., 2015 [22]		MODIS/AVHRR NDVI		1981–2006	−0.01
Nayak et al., 2016 [63]		NDVI		2001–2006	−0.042 ± 0.02
Gahlot et al., 2017 [64]		-		2000–2017	−0.02
Raju et al., 2023 [62]		Eddy covariance flux		2011–2020	−0.16 ± 0.02
Ravi et al. 2023 [23]		MODIS, OCO-2, TROPOMI SIF		2012–2020	-0.38 to −0.53

5.4. Analysis of Simulated and Observed Concentrations

The model captures the variability over the region and hence represents the seasonal cycle for several sites, namely GAD, MOH, and PUN (Figure 4). NTL, the background site, has lesser influence from fossil emissions, but the model has difficulty representing the variability over the region due to the complex orography and wind pattern. As the representation of local meteorological factors in the model has a crucial influence on the representation of the seasonal cycle, the model captures the summer variability at this site, while the winter variations are partially reproduced. For MOH and GAD, the model clearly explains the variability over the region, but the data (MOH) are not long enough to check the model's fit for the entire study period.

GAD, though a rural site, is influenced by the fossil fuel emissions generated by local traffic and the human activities required to sustain life. The emissions from other regions are also transported to this region, as the site is under the strong influence of Indian monsoonal winds. The model represents a seasonal cycle that is similar to the observations. Over PUN, the overall model performance is good, but the winter variability is better reproduced compared to the summer seasons. The model captures the fossil emissions that are generated by local anthropogenic activity over the region. The variability over CLA is only partially represented by the model and a large misfit can be noticed.

The correlation between the observed and the simulated values is given in Table 4. The correlation is increased upon optimization. The highest correlation is obtained for PUN followed by NTL, and the lowest correlation is for CLA, which indicates that the model could not simulate the variability at this site.

Table 4. The correlation between the observed and simulated CO_2 concentration for four Indian sites and Comilla, Bangladesh.

Station	Prior ppm	Optim. ISG ppm
CLA	0.76	0.76
GAD	0.83	0.91

Table 4. *Cont.*

Station	Prior ppm	Optim. ISG ppm
MOH	0.77	0.82
NTL	0.82	0.85
PUN	0.87	0.90

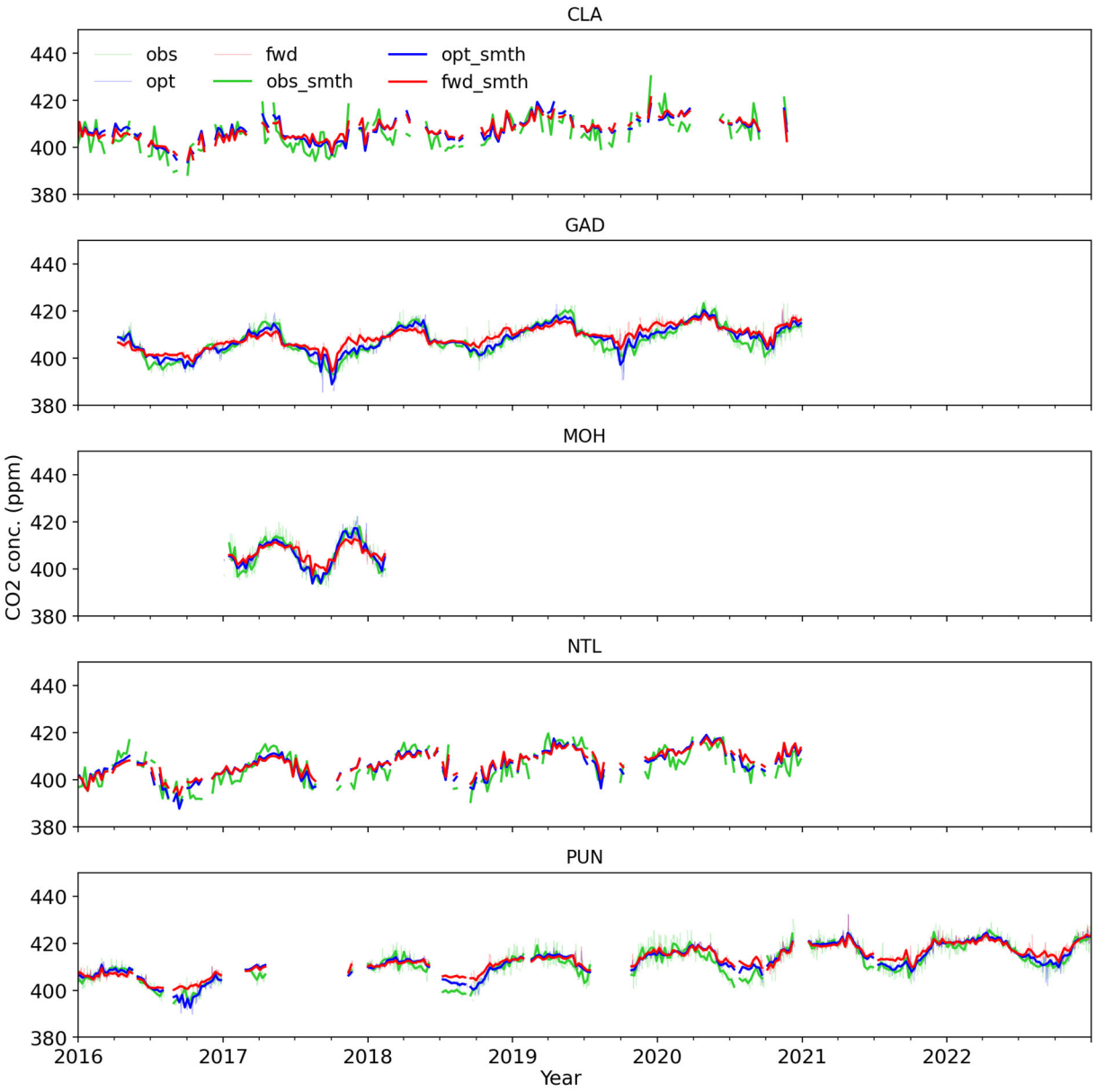

Figure 4. Time series of observed (obs), forward (fwd, with prior fluxes), and inversion-optimized (opt) CO_2 concentration for the four Indian sites and Comilla, Bangladesh. The smoothed values are the weekly averages of daily measures.

5.5. Model Error Statistics for the Indian Sub-Continental Measurements

The average bias from the Indian sub-continental sites (Figure 5) is lower for ISG compared to ISGH and I4SG (Table 5). Here, BIAS is represented as the average of the model–observation difference; hence, a positive bias implies that the model estimates are higher than the observations and vice versa. However, a reduced bias was noticed for ISG throughout the year, and the bias of I4SG was generally higher than that for ISG. Although

ISGH is improved compared to ISG in a few months, the larger biases are still obvious. Thus, a reduced bias over Indian sub-continental sites is obtained from ISG, though a large difference in bias was not noticed from case to case. The RMSE for each site in Table 6 shows an overall improvement in ISG.

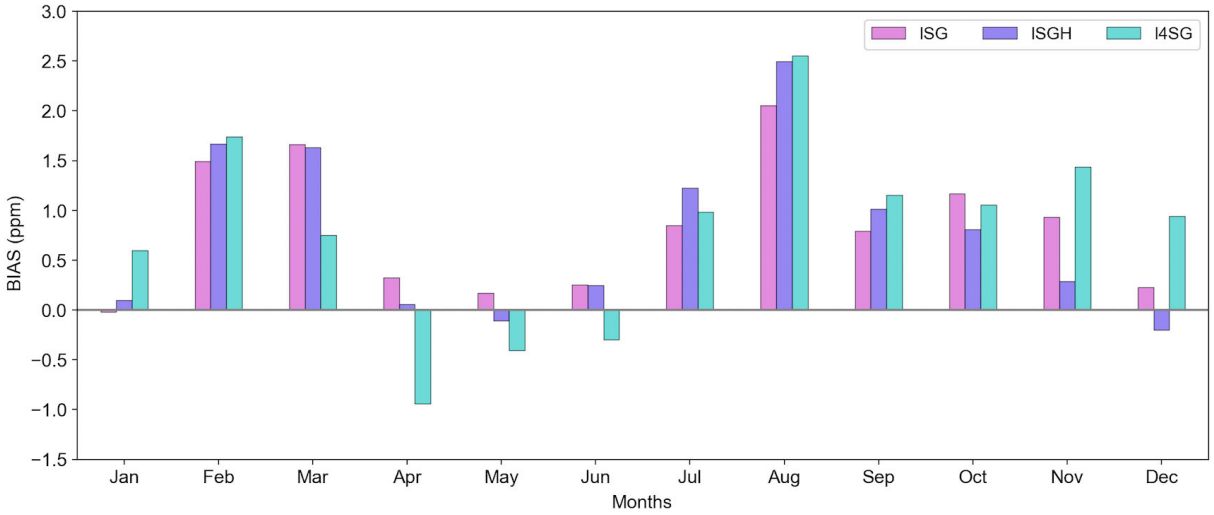

Figure 5. Monthly BIAS averaged for all Indian sites and Comilla (unit is ppm).

Table 5. Bias for Indian sub-continental sites from the inversions ISG, ISGH, and I4SG (unit is ppm).

Station	Prior	ISG	ISGH	I4SG
CLA	1.65	1.65	1.35	-
GAD	1.11	0.35	0.40	0.47
MOH	0.24	0.15	−0.06	0.34
NTL	1.46	0.89	1.02	1.05
PUN	1.37	0.80	0.83	0.83

Table 6. RMSE for Indian sub-continental sites from inversions ISG, ISGH, and I4SG (unit is ppm).

Station	Prior	ISG	ISGH	I4SG
CLA	4.62	4.60	4.67	-
GAD	3.85	2.73	2.86	2.83
MOH	4.46	3.77	3.90	3.80
NTL	4.30	3.83	3.87	3.86
PUN	3.90	3.29	3.34	3.35

The monthly bias for each of the Indian sub-continental sites is shown in Figure 6. The bias of inversion ISG is overall reduced compared to inversion ISGH. CLA has a prominent bias throughout the year, whereas NTL has a large winter bias. The summer bias is high for PUN and GAD, while spring biases are high for MOH.

The monthly bias for the GOSAT measurements is given in Figure 7. The bias is averaged for each 10° latitude band. Over the tropics, the average bias is within ±0.01 ppm, whereas a positive bias is dominant for the higher latitudes (north of 30°N). The bias south of 30°S is smaller than the bias in the higher latitudes of the Northern Hemisphere.

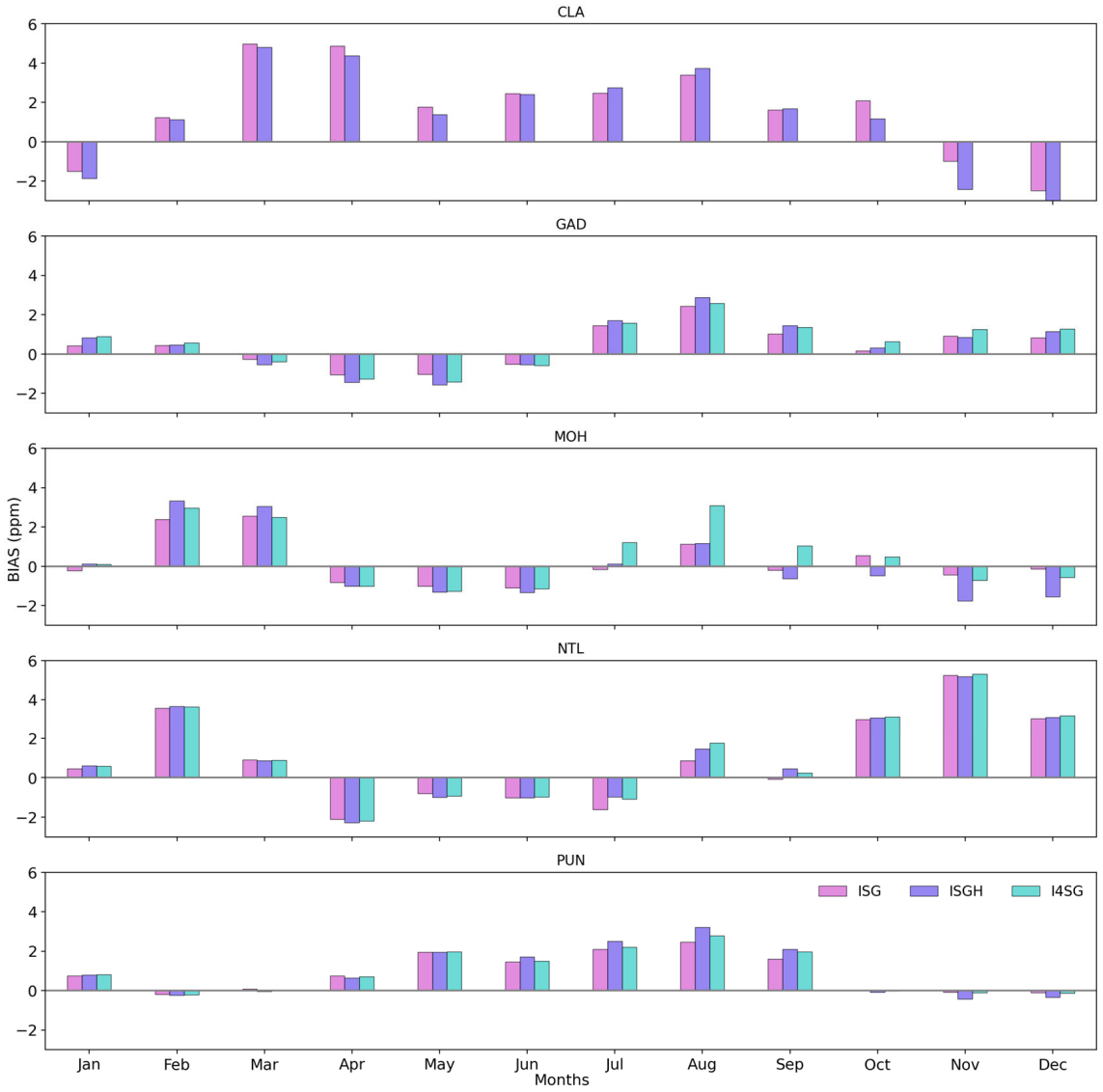

Figure 6. Monthly bias for each Indian site and Comilla from inversions ISG, ISGH, and I4SG (unit ppm).

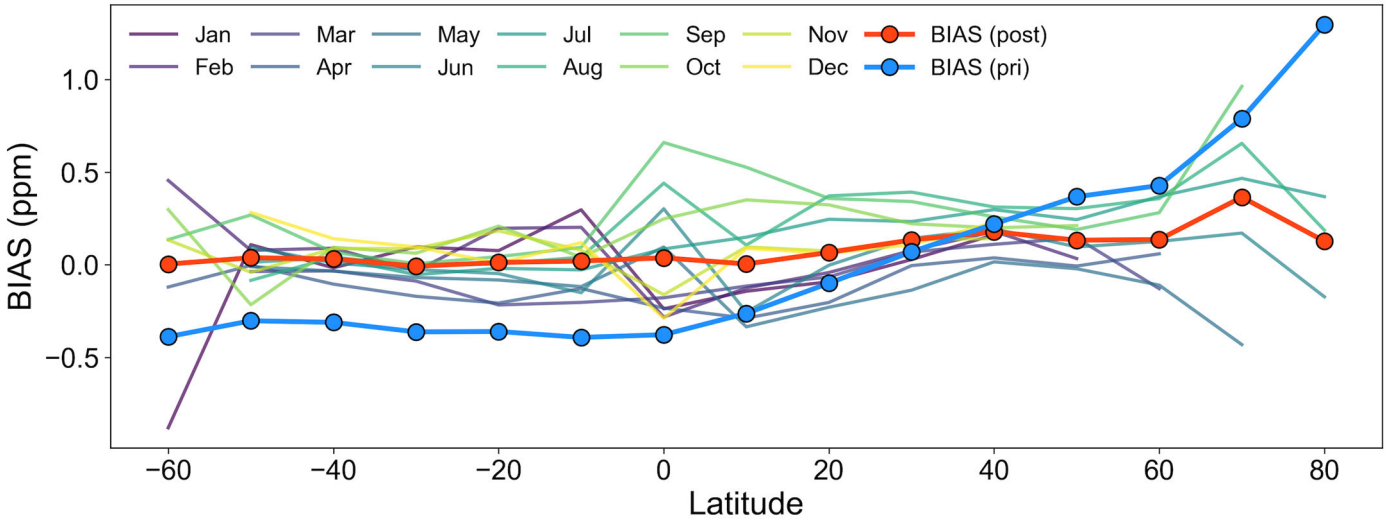

Figure 7. The monthly posterior bias of GOSAT measurements averaged for each 10° latitude bin obtained from inversion ISG (unit ppm). The latitude given in the x-axis is the lower limit of each 10° bin.

5.6. Evaluation with Independent Measurements

The smoothed values are the weekly averages of the daily measures. The measurements from the SNG were not included in the inversions and hence used to validate the outputs from the inversions. The comparison with the observed concentration is reasonable for this site, though the site does not have a longer record (Figure 8). The seasonal variability during the latter half of the year is better simulated by the model than in the spring and summer seasons. This improvement could be due to the joint contribution of the surface and GOSAT satellite measurements, as the observation density of satellite measurement increases during the cloud-free fall and winter seasons.

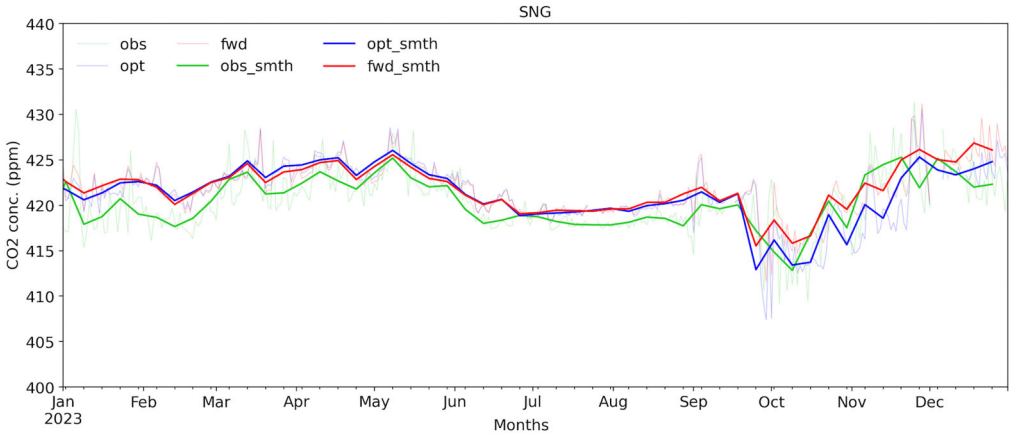

Figure 8. Same plots as Figure 4 but for SNG validation site.

6. Discussion

The global terrestrial biospheric flux plays a significant role in the entire carbon cycle. These sinks curb the drastic increase in the global temperature by absorbing the increasing anthropogenic CO_2 emissions [65]. A reasonable estimation of biospheric fluxes at global and regional scales enables a deeper understanding of the carbon cycle, though the unavailability of observations poses a challenge. For top-down estimates, ground-based observations provide valuable information for constraining fluxes, especially in regions where satellite-based observations have limitations due to cloud cover.

In this study, an attempt has been made to estimate the terrestrial biospheric fluxes over India by assimilating the measurements from GOSAT and global surface sites, and assimilating additional measurements from the NIES database, vertical CO_2 profiles from Brazil, and the Indian surface network in a global inverse model. The model optimizes terrestrial biosphere and ocean–atmosphere exchanges independently to produce the terrestrial biospheric fluxes over large land and ocean regions. The flux estimates are obtained by combining data from multiple platforms over India, and such estimates are more reliable as they are based on numerous observations. Including denser observations will allow the model to give corrections in regions with notable CO_2 variability and avoid producing irrelevant adjustments. Thus, the CO_2 flux estimate obtained by the inverse model over the South Asian region was found to be -0.23 PgC yr^{-1}, which is within the OCO-2 multi-model spread (-0.35 to 0.2 PgC yr^{-1}) and is in good agreement with the estimates from several other studies that show South Asia to be a sink (-0.104 ± 0.15 PgC yr^{-1}, [66]; -0.02 ± 0.17 PgC yr^{-1} [12]). A similar study by [58] also confirmed that South Asia is a sink (-0.25 ± 0.11 PgC yr^{-1}) for the period 2000–2009 by including lateral carbon transport.

The impact of adding observations from the Indian subcontinent to the inversions was assessed. In our inversions, we used different model parameters, as detailed in Table 2, and estimated that the mean flux over India is -0.147 ± 0.09 PgC yr^{-1} (sink), using the measurements from GOSAT, global surface, regional and Indian sites; however, the estimate

was lower (reduced sink) in inversions with increased observation uncertainty (reduced weight) for GOSAT measurements. Even though higher uncertainty offers larger freedom for fitting the measurements in the model, the reduction in the sink could be due to the stricter filtering of the GOSAT measurements, by which more observations are discarded during the inversions. This indicates that GOSAT measurements also constrain the model fluxes, along with the Indian sub-continental measurements, and hence play a crucial role in modulating the flux estimates over the Indian region. In the absence of Indian sub-continental measurements, all the inversions gave a reduced sink; an even weaker sink was obtained in inversions with larger uncertainty (reduced weight of) for GOSAT measurements. Here, GOSAT measurements have more freedom to counterbalance the South Asian sink elsewhere, as the model is not constrained by the Indian sub-continental measurements. However, our estimate of a near-neutral value of 0.040 ± 0.133 PgC yr^{-1} over India using the GOSAT and ObsPack datasets (without Indian sub-continental measurements) is comparable to the estimates of -0.04 ± 0.14 PgC yr^{-1} reported by [5] over South Asia using the measurements from the OCO-2 and ObsPack dataset. These estimates are comparable in spite of the differences in the extent of their land area; this is because a major part of South Asian emissions is contributed by India. It is also notable that the uncertainty in the estimates is reduced by including the measurements from the Indian subcontinent.

It is worth comparing our fluxes over India to some previous studies. The estimate obtained from an ensemble of CO_2 inverse models [16] for the years 2016 to 2019 ranges from -0.333 PgC yr^{-1} to 0.146 PgC yr^{-1}. Our total flux of -0.147 ± 0.09 PgC yr^{-1} for the period 2016–2023 is within the range of this ensemble and thus comparable. The flux estimates from 2015 to 2021 indicate that India is a carbon sink (-0.065 ± 0.02 PgC yr^{-1}; [60]); meanwhile, the median of the ensemble for the year 2020 indicates that it is a source (0.091 PgC yr^{-1}). However, due to the higher CO_2 variability over the region [25,29], studies also incorporate surface observations from India in inversions [18,21], which have more consistent data records than remotely sensed data, especially in the regions with higher convective activity. In general, the year-to-year flux estimates from our inversions suggest that India is a carbon sink.

It is well known that there exist considerable differences between the bottom-up and top-down estimates. Though bottom-up fluxes suggest India to be a source region during the period 1901–2010 [67], other studies suggest a near-neutral flux in the early 2000s [22,63]. However, some studies have reported that India is a carbon sink in recent years [23,62]. The results of top-down estimates also depend on the observation used, either using surface-only or a combination of surface and remote sensing data. The net flux evolved into a stronger sink when using only Indian surface CO_2 observations or a combination of surface and satellite observations over India [18,21]; however, it turned out to be neutral when using only global ground-based measurements [68] in inversions. The estimates obtained using satellite measurements were also similar, but the uncertainty was comparable to the fluxes. These uncertainties in the estimation of fluxes could be due to partial observations from satellites, as cloud cover and aerosols influence the satellite measurements. Similarly, the ground measurements obtained from ObsPack datasets do not cover the entire land region of India and may not completely explain the variability, as the CO_2 measurements over the country have large spatiotemporal variability [25,29]. Therefore, remotely sensed, aircraft, or surface measurements, the spatial coverage, and the number of measurements is critical in inverse modeling [69]. Thus, from a combination of measurements obtained from the Indian subcontinent, global surface, and GOSAT measurements, our inversions produced a noticeable sink (-0.147 ± 0.09 PgC yr^{-1}) over the Indian region, as the model is constrained by the observations from a regional network. This helps the model to capture

the strong CO_2 variability arising from the various phenomena over India, such as the monsoons (SW and NE), El Niño, and complex orography, and to produce reasonable estimates that could be lacking inversions without Indian sub-continental measurements.

The improvement observed when including Indian sub-continental measurements has also been evaluated. The bias and RMSE at Indian sites were found to be reduced in inversions with Indian sub-continental measurements compared to inversions without Indian sub-continental measurements. The correlations also increased at each site. The seasonal variation at each site improved due to flux corrections by the inverse model, and the model's fit to observations was notably improved at sites with anthropogenic influences (GAD, PUN, and MOH). The variability at the background site, NTL, was not fully reproduced, which could be due to the complex orography and wind pattern experienced at the site, and possibly due to the weak summer uptake in the prior fluxes. Similarly, the simulated and observed CO_2 concentrations at CLA have a weaker correlation. The CLA site is known to be difficult to simulate, especially at low wind conditions, leading to large biases in the observation; therefore, the model tries to reject the observations, considering them to be outliers. To handle this, we give high uncertainty to CLA measurements (9 ppm). Even then, the model is not properly constrained by the site's observation.

In addition to the limited availability of observational data in the public domain, estimating the biospheric CO_2 fluxes over India remains challenging due to other conditions, such as the complex topography, strong and variable biospheric fluxes, and the influence of large-scale phenomena like monsoons. Efforts to understand the terrestrial biospheric exchanges are further restricted by the representation of the meteorology in the model and the understanding of underlying processes. The inadequacy of observation coverage for the region also hinders further developments in the estimation of emissions. Therefore, including denser and more consistent observations from surface, aircraft or remote sensing networks is essential for the robust estimation of terrestrial biospheric fluxes in this region. While satellite observations have attempted to fill the gaps in data-sparse regions, the surface networks provide foundational data and are particularly necessary in regions with high convective activity, as the cloud cover poses a difficulty to the current satellite missions.

Satellite measurements also undergo rigorous filtering to ensure the quality of the data products, as they can be affected by cloud cover and aerosols. However, this filtering process can result in data loss, making it challenging to fully capture the seasonal cycle. Effective solutions would be to obtain ample measurements in both time and space and employ newer techniques and instruments to achieve accurate observations, even under cloudy conditions. This approach would ensure sufficient data availability and reduce biases in satellite products, ultimately enhancing our understanding of the underlying physics and facilitating the accurate estimation of sinks and sources at national and subnational levels.

7. Conclusions

We used a global high-resolution inverse model, NIES-TM-FLEXPART-VAR (NTF-VAR), to estimate biospheric CO_2 fluxes over India by assimilating measurements from surface networks, GOSAT satellite, and vertical CO_2 profiles from Brazil. The inverse model optimized terrestrial biosphere and ocean–atmosphere exchanges independently and estimated the land biospheric fluxes across the South Asia region, including India. The estimated South Asian biospheric flux (-0.23 PgC yr^{-1}), which was obtained by integrating measurement data from the Indian subcontinent region, is comparable to the multi-model estimate obtained from the OCO-2 intercomparison projects (-0.35 to 0.20 PgC yr^{-1}). Without the Indian subcontinent measurement data, our estimate indicated a weaker sink of 0.12 PgC yr^{-1}. For India, our inversions, which assimilated surface observations from the

Indian subcontinent region, yielded a significant sink of 0.147 ± 0.094 PgC yr^{-1}. In contrast, without including the observations, the estimated flux value shifted to a neutral value of 0.040 ± 0.133 PgC yr^{-1}. The inversion with the stricter filtering of GOSAT observations also resulted in a reduced biospheric CO_2 flux over the India and South Asia region being estimated. Therefore, our result suggested that combining surface measurements from the Indian subcontinent with GOSAT data could be beneficial for constraining the flux inverse model and achieving robust flux estimates. The estimated fluxes were validated against independent observational data from the Sinhagad site. The close agreement between the model predictions and the observed concentrations suggests that the model estimates are reasonable. However, we note that achieving precise flux estimates will further require much denser observations from various platforms.

Supplementary Materials: The details of the observation sites used in this study are included. The following supporting information can be downloaded at: https://www.mdpi.com/article/10.3390/rs17030450/s1, Table S1. Details of surface/aircraft sites used in the study.

Author Contributions: Conceptualization, S.M.; Methodology, L.N. and S.M.; Software, L.N., S.M. and R.J.; Validation, L.N. and S.M.; Formal analysis, L.N. and S.M.; Investigation, L.N. and S.M.; Resources, T.M.; Data curation, L.N., S.M., T.O., Y.K.T., G.S., A.D., C.D.J., M.V.R., V.S., H.H., Y.T., M.N., M.K.A., H.M., J.Z., J.W.K., Y.S. and Y.Y.; Writing—original draft, L.N.; Writing—review & editing, S.M., R.J., T.O., Y.K.T., C.D.J., H.H., Y.T., J.W.K. and Y.Y.; Visualization, L.N. and R.J.; Supervision, S.M.; Project administration, T.M.; Funding acquisition, T.M. All authors have read and agreed to the published version of the manuscript.

Funding: This study was financially supported by NIES GOSAT and GOSAT-2 projects and Ministry of the Environment, Japan. TO is supported by the NASA grants 80NSSC21K1929 and 80NSSC25K7212.

Data Availability Statement: Some of the datasets presented in this article are not readily available because of administrative restrictions. Requests to access the datasets should be directed to the corresponding observational data contributors. Prior fluxes: Biomass burning: Biomass burning GFAS —https://www.ecmwf.int/en/forecasts/dataset/global-fire-assimilation-system (accessed on 18 June 2024). ODIAC (version 2020, 2022)—www.nies.go.jp/doi/10.17595/20170411.001-e.html (accessed on 28 June 2022). Ocean Flux—www.nies.go.jp/doi/10.17595/20201020.001-e.html (accessed on 7 May 2021). Vegetation uptake, respiration—www.nies.go.jp/doi/10.17595/20200227.001-e.html (accessed on 9 March 2020). CO_2 observations: CLA—DOI:10.17595/20220301.002 (accessed on 26 April 2024). COI—DOI:10.17595/20160901.002 (accessed on 4 June 2024). HAT—DOI:10.17595/20160901.001 (accessed on 4 June 2024). MFJ—DOI:10.17595/20170616.001 (accessed on 4 June 2024). NTL—DOI:10.17595/20220301.001 (accessed on 26 April 2024). ALT, SAN and TEF—https://doi.pangaea.de/10.1594/PANGAEA.926834, https://doi.org/10.1594/PANGAEA.949643 (accessed on 4 June 2024). ObsPack—http://doi.org/10.25925/20231201 (accessed on 12 December 2023), http://doi.org/10.25925/20240215 (accessed on 27 March 2024). GOSAT- https://data2.gosat.nies.go.jp/ (accessed on 13 June 2024). Model comparison: OCO-2 v10 MIP gridded fluxes (IS) —https://gml.noaa.gov/ccgg/OCO2_v10mip/ (accessed on 20 Sep 2023).

Acknowledgments: The authors thank the National Institute for Environmental Studies, Japan, for providing the supercomputer facility to carry out all simulations in this work. The authors also acknowledge the funding from the GOSAT project of NIES, Japan. TO is supported by the NASA grants 80NSSC21K1929 and 80NSSC25K7212. We thank all the data contributors of the ObsPack Dataset. We thank A. Andrews (NOAA), D. Kubustin (DWD), S. O'Doherty (UOB), A. Hensen (ECN), L. Haszpra (ATOMKI), J. Levula (UHELS), M. Leuenberger (KUP), M. Molder (LUND–NATEKO), A. Lindroth (LU), A. Hoheisel (HU), K. Lehtinen (UEF), M. Heliasz (LU), M. Lopez (LSCE), Marcus Schumacher (DWD), Pierre-Eric Blanc (OSUpytheas), G. Vitkova (Czech Globe), C. Labuschagne (SAWS), B. Scheeren (RUG), J. A. Morgui (ICTA–UAB), C. Couret (HU), E. Kozlova (UOEX), J. Hatakka (FMI) and C. Gerbig (MPI-BGC) for supplying the tower in situ datasets. We thank K. Thoning

(NOAA), M. Ramonet (LSCE), B. Stephens (UCAR), P. Cristofanelli (ISAC–CNR), G. Forster (UEA), S. Henne (Empa), G. Brailsford (NIWA), L. V. Gatti of (INPE), J. Necki (AGH), S. C. Biraud (LBNL–ARM), F. Apadula (RSE), A.G. di Sarra (ENEA), T. Laurila (FMI), Prinzivalli S (EarthNetworks), D. Martin (NUI), S. Morimoto (TU), P. P. Rivas (AEMET), C. L. Myhre (NILU) and S. Takatsuji (JMA) for collecting the surface in situ datasets. We thank B. Law (OSU), M. Delmotte (LSCE) and C. Sweeney (NOAA) for providing the surface and tower datasets, and J. B. Miller (NOAA) for the PFP measurements. We give special thanks to Y. Nojiri (NIES) for the shipboard measurements and M. Sasakawa (NIES) for the tower in situ measurements over Siberia, Russia. We acknowledge R. Langenfelds (CSIRO) and R. Keeling, (SIO) for contributing datasets from different parts of the world. We are thankful to Doug Worthy (ECCC) for the surface in situ datasets from the 17 sites in Canada and are grateful to Xin Lan (NOAA) and colleagues for contributing the flask, tower, and PFP measurements (60 sites) across the globe. We acknowledge the use of OCO-2 MIP flux datasets for model comparisons and GFAS data in this study (GFAS data were generated using Copernicus Atmosphere Monitoring Service Information 2021). We thank Krishnan, of Indian Institute of Tropical Meteorology (IITM), Pune, Ministry of Earth Sciences, Govt. of India, for supporting the GHG observations at Sinhagad (SNG) and Pune (PUN). We thank the Department of Space, Government of India, for their financial support during this work through the ISRO-GBP ATCTM project for Gadanki Measurements. We acknowledge L.V. Gatti for the aircraft measurements from three sites over the Amazon, Brazil.

Conflicts of Interest: The authors declare no conflicts of interest.

References

1. Friedlingstein, P.; Jones, M.W.; O'Sullivan, M.; Andrew, R.M.; Hauck, J.; Peters, G.P.; Peters, W.; Pongratz, J.; Sitch, S.; Le Quéré, C.; et al. Global Carbon Budget 2019. *Earth Syst. Sci. Data* **2019**, *11*, 1783–1838. [CrossRef]
2. ADO. *Asia in the Global Transition to Net Zero*; Asian Development Outlook 2023 Thematic Report; Asian Development Bank: Manila, Philippines, 2023.
3. Patra, P.K.; Houweling, S.; Krol, M.; Bousquet, P.; Belikov, D.; Bergmann, D.; Bian, H.; Cameron-Smith, P.; Chipperfield, M.P.; Corbin, K.; et al. TransCom model simulations of CH4 and related species: Linking transport, surface flux and chemical loss with CH4 variability in the troposphere and lower stratosphere. *Atmos. Chem. Phys.* **2011**, *11*, 12813–12837. [CrossRef]
4. Thompson, R.L.; Patra, P.K.; Chevallier, F.; Maksyutov, S.; Law, R.M.; Ziehn, T.; Van Der Laan-Luijkx, I.T.; Peters, W.; Ganshin, A.; Zhuravlev, R.; et al. Top-down assessment of the Asian carbon budget since the mid 1990s. *Nat. Commun.* **2016**, *7*, 10724. [CrossRef]
5. Philip, S.; Johnson, M.S.; Baker, D.F.; Basu, S.; Tiwari, Y.K.; Indira, N.K.; Ramonet, M.; Poulter, B. OCO-2 Satellite-Imposed Constraints on Terrestrial Biospheric CO_2 Fluxes Over South Asia. *J. Geophys. Res. Atmos.* **2022**, *127*, e2021JD035035. [CrossRef]
6. National Academies of Sciences, Engineering, and Medicine (NASEM). *Greenhouse Gas Emissions Information for Decision Making: A Framework Going Forward.*; The National Academies Press: Washington, DC, USA, 2022; p. 510.
7. Gurney, K.R.; Law, R.M.; Denning, A.S.; Rayner, P.J.; Baker, D.; Bousquet, P.; Bruhwiler, L.; Chen, Y.H.; Ciais, P.; Fan, S.; et al. TransCom 3 CO2inversion intercomparison: 1. Annual mean control results and sensitivity to transport and prior flux information. *Tellus Ser. B Chem. Phys. Meteorol.* **2003**, *55*, 555–579. [CrossRef]
8. Gurney, K.R.; Law, R.M.; Denning, A.S.; Rayner, P.J.; Pak, B.C.; Baker, D.; Bousquet, P.; Bruhwiler, L.; Chen, Y.-H.; Ciais, P.; et al. Transcom 3 inversion intercomparison: Model mean results for the estimation of seasonal carbon sources and sinks. *Glob. Biogeochem. Cycles* **2004**, *18*, 1–18. [CrossRef]
9. Maksyutov, S.; Machida, T.; Mukai, H.; Patra, P.K. Effect of recent observations on Asian CO_2 flux. *Tellus B Chem. Phys. Meteorol.* **2003**, *55*, 522–529. [CrossRef]
10. Maksyutov, S.; Takagi, H.; Valsala, V.K.; Saito, M.; Oda, T.; Saeki, T.; Belikov, D.A.; Saito, R.; Ito, A.; Yoshida, Y.; et al. Regional CO_2 flux estimates for 2009-2010 based on GOSAT and ground-based CO_2 observations. *Atmos. Chem. Phys.* **2013**, *13*, 9351–9373. [CrossRef]
11. Takagi, H.; Saeki, T.; Oda, T.; Saito, M.; Valsala, V.; Belikov, D.; Saito, R.; Yoshida, Y.; Morino, I.; Uchino, O.; et al. On the Benefit of GOSAT Observations to the Estimation of Regional CO_2 Fluxes. *Sola* **2011**, *7*, 161–164. [CrossRef]
12. Cervarich, M.; Shu, S.; Jain, A.K.; Arneth, A.; Canadell, J.; Friedlingstein, P.; Houghton, R.A.; Kato, E.; Koven, C.; Patra, P.; et al. The terrestrial carbon budget of South and Southeast Asia. *Environ. Res. Lett.* **2016**, *11*, 105006. [CrossRef]
13. Patra, P.K.; Saeki, T.; Dlugokencky, E.J.; Ishijima, K.; Umezawa, T.; Ito, A.; Aoki, S.; Morimoto, S.; Kort, E.A.; Crotwell, A.; et al. Regional Methane Emission Estimation Based on Observed Atmospheric Concentrations (2002–2012). *J. Meteorol. Soc. Jpn.* **2016**, *94*, 85–113. [CrossRef]

14. Byrne, B.; Jones, D.B.A.; Strong, K.; Zeng, Z.-C.; Deng, F.; Liu, J. Sensitivity of CO_2 surface flux constraints to observational coverage. *J. Geophys. Res. Atmos.* **2017**, *122*, 6672–6694. [CrossRef]
15. Byrne, B.; Baker, D.F.; Basu, S.; Bertolacci, M.; Bowman, K.W.; Carroll, D.; Chatterjee, A.; Chevallier, F.; Ciais, P.; Cressie, N.; et al. National CO_2 budgets (2015–2020) inferred from atmospheric CO_2 observations in support of the Global Stocktake. *Earth Syst. Sci. Data Discuss.* **2022**, *2022*, 1–59. [CrossRef]
16. Deng, Z.; Ciais, P.; Tzompa-Sosa, Z.A.; Saunois, M.; Qiu, C.; Tan, C.; Sun, T.; Ke, P.; Cui, Y.; Tanaka, K.; et al. Comparing national greenhouse gas budgets reported in UNFCCC inventories against atmospheric inversions. *Earth Syst. Sci. Data* **2022**, *14*, 1639–1675. [CrossRef]
17. Basu, S.; Lehman, S.J.; Miller, J.B.; Andrews, A.E.; Sweeney, C.; Gurney, K.R.; Xu, X.; Southon, J.; Tans, P.P. Estimating US fossil fuel CO_2 emissions from measurements of 14C in atmospheric CO_2. *Proc. Natl. Acad. Sci. USA* **2020**, *117*, 13300–13307. [CrossRef]
18. Halder, S.; Tiwari, Y.K.; Valsala, V.; Sijikumar, S.; Janardanan, R.; Maksyutov, S. Benefits of satellite XCO_2 and newly proposed atmospheric CO_2 observation network over India in constraining regional CO_2 fluxes. *Sci. Total Environ.* **2022**, *812*, 151508. [CrossRef]
19. Nalini, K.; Sijikumar, S.; Valsala, V.; Tiwari, Y.K.; Ramachandran, R. Designing surface CO_2 monitoring network to constrain the Indian land fluxes. *Atmos. Environ.* **2019**, *218*, 117003. [CrossRef]
20. Sijikumar, S.; Raju, A.; Valsala, V.; Tiwari, Y.; Girach, I.A.; Jain, C.D.; Ratnam, M.V. High-Resolution Bayesian Inversion of Carbon Dioxide Flux Over Peninsular India. *Atmos. Environ.* **2023**, *308*, 119868. [CrossRef]
21. Swathi, P.S.; Indira, N.K.; Ramonet, M. Estimation of Carbon Dioxide Fluxes Between Land, Ocean and Atmosphere During 2006–2011 with a 4D Variational Assimilation Scheme and Special Reference to Asia. In *Climate Change and Green Chemistry of CO_2 Sequestration*; Goel, M., Satyanarayana, T., Sudhakar, M., Agrawal, D.P., Eds.; Springer Singapore: Singapore, 2021; pp. 289–310. ISBN 978-981-16-0029-6.
22. Nayak, R.K.; Patel, N.R.; Dadhwal, V.K. Spatio-temporal variability of net ecosystem productivity over India and its relationship to climatic variables. *Environ. Earth Sci.* **2015**, *74*, 1743–1753. [CrossRef]
23. Ravi, A.; Pillai, D.; Gerbig, C.; Sitch, S.; Zaehle, S.; Thilakan, V.; Jha, C.S. Spatiotemporal variations in terrestrial biospheric CO_2 fluxes of India derived from MODIS, OCO-2 and TROPOMI satellite observations and a diagnostic terrestrial vegetation model. *EGUsphere* **2023**, *2023*, 1–69. [CrossRef]
24. Jain, C.D.; Singh, V.; Raj, S.T.A.; Madhavan, B.L.; Ratnam, M.V. Local emission and long-range transport impacts on the CO, CO_2, and CH4 concentrations at a tropical rural site. *Atmos. Environ.* **2021**, *254*, 118397. [CrossRef]
25. Krishnapriya, M.; Nayak, R.K.; Allahudeen, S.; Bhuvanachandra, A.; Dadhwal, V.K.; Jha, C.S.; Sheshasai, M.V.R.; Sasmal, S.K.; Prasad, K.V.S.R. Seasonal variability of tropospheric CO_2 over India based on model simulation, satellite retrieval and in-situ observation. *J. Earth Syst. Sci.* **2020**, *129*, 211. [CrossRef]
26. Liu, Y.; Gruber, N.; Brunner, D. Spatiotemporal patterns of the fossil-fuel CO_2 signal in central Europe: Results from a high-resolution atmospheric transport model. *Atmos. Chem. Phys.* **2017**, *17*, 14145–14169. [CrossRef]
27. Pathakoti, M.; Mahalakshmi, D.V.; Gaddamidi, S.; Arun, S.S.; Bothale, R.V.; Chauhan, P.; Raja, P.; Rajan, K.S.; Chandra, N. Three-dimensional view of CO_2 variability in the atmosphere over the Indian region. *Atmos. Res.* **2023**, *290*, 106785. [CrossRef]
28. Ravi Kumar, K.; Valsala, V.; Tiwari, Y.K.; Revadekar, J.V.; Pillai, P.; Chakraborty, S.; Murtugudde, R. Intra-seasonal variability of atmospheric CO_2 concentrations over India during summer monsoons. *Atmos. Environ.* **2016**, *142*, 229–237. [CrossRef]
29. Thilakan, V.; Pillai, D.; Sukumaran, J.; Gerbig, C.; Hakkim, H.; Sinha, V.; Terao, Y.; Naja, M.; Deshpande, M.V. Potential of using CO_2 observations over India in a regional carbon budget estimation by improving the modelling system. *Atmos. Chem. Phys.* **2024**, *24*, 5315–5335. [CrossRef]
30. Maksyutov, S.; Oda, T.; Saito, M.; Janardanan, R.; Belikov, D.; Kaiser, J.W.; Zhuravlev, R.; Ganshin, A.; Valsala, V.K.; Andrews, A.; et al. Technical note: A high-resolution inverse modelling technique for estimating surface\chemCO_2 fluxes based on the NIES-TM–FLEXPART coupled transport model and its adjoint. *Atmos. Chem. Phys.* **2021**, *21*, 1245–1266. [CrossRef]
31. Schuldt, K.N.; Mund, J.; Aalto, T.; Abshire, J.B.; Aikin, K.; Allen, G.; Arlyn, A.; Apadula, F.; Arnold, S.; Baier, B.; et al. Multi-Laboratory Compilation of Atmospheric Carbon Dioxide Data for the Period 1957–2022. 2023. Available online: https://gml.noaa.gov/ccgg/obspack/data.php?id=obspack_co2_1_GLOBALVIEWplus_v9.1_2023-12-08 (accessed on 12 December 2023).
32. Schuldt, K.N.; Jacobson, A.R.; Aalto, T.; Arlyn, A.; Apadula, F.; Arnold, S.; Bakwin, P.; Bäni, L.; Bartyzel, J.; Bergamaschi, P.; et al. Multi-Laboratory Compilation of Atmospheric Carbon Dioxide Data for the Years 2023–2024. 2024. Available online: https://gml.noaa.gov/ccgg/obspack/data.php?id=obspack_co2_1_NRT_v9.2_2024-03-25 (accessed on 27 March 2024).
33. Nomura, S.; Naja, M.; Ahmed, M.K.; Mukai, H.; Terao, Y.; Machida, T.; Sasakawa, M.; Patra, P.K. Measurement report: Regional characteristics of seasonal and long-term variations in greenhouse gases at Nainital, India, and Comilla, Bangladesh. *Atmos. Chem. Phys.* **2021**, *21*, 16427–16452. [CrossRef]

34. Terao, Y.; Nomura, S.; Mukai, H.; Machida, T.; Sasakawa, M.; Naja, M. Atmospheric Carbon Dioxide Dry Air Mole Fraction at Nainital, India. 2022. Ver. 2022.01. Available online: https://www.nies.go.jp/doi/10.17595/20220301.001-e.html (accessed on 26 April 2024).
35. Belikov, D.A.; Saitoh, N.; Patra, P.K.; Chandra, N. GOSAT CH4 Vertical Profiles over the Indian Subcontinent: Effect of a Priori and Averaging Kernels for Climate Applications. *Remote Sens.* **2021**, *13*, 1677. [CrossRef]
36. Sinha, V.; Kumar, V.; Sarkar, C. Chemical composition of pre-monsoon air in the Indo-Gangetic Plain measured using a new air quality facility and PTR-MS: High surface ozone and strong influence of biomass burning. *Atmos. Chem. Phys.* **2014**, *14*, 5921–5941. [CrossRef]
37. Metya, A.; Datye, A.; Chakraborty, S.; Tiwari, Y.K.; Patra, P.K.; Murkute, C. Methane sources from waste and natural gas sectors detected in Pune, India, by concentration and isotopic analysis. *Sci. Total Environ.* **2022**, *842*, 156721. [CrossRef]
38. Mukai, H. Continuous Observational Data of Atmospheric CO2 Mixing Ratios on Cape Ochi-ishi, Ver. 1.2, 2014. Available online: https://www.nies.go.jp/doi/10.17595/20160901.002-e.html (accessed on 4 June 2024).
39. Mukai, H. Continuous Observational Data of Atmospheric CO2 Mixing Ratios on Hateruma Island, Ver. 1.5, 2014. Available online: https://www.nies.go.jp/doi/10.17595/20160901.001-e.html (accessed on 4 June 2024).
40. Nomura, S. Daily Observational Data of Atmospheric CO2 Mixing Ratios at the Summit of Mt. Fuji. 2017. Available online: https://www.nies.go.jp/doi/10.17595/20170616.001-e.html (accessed on 4 June 2024).
41. Gatti, L.V.; Correa, C.C.S.; Domingues, L.G.; Miller, J.B.; Gloor, M.; Martinewski, A.; Basso, L.S.; Santana, R.; Crispim, S.P.; Marani, L.; et al. CO2 Vertical Profiles on Four Sites over Amazon from 2010 to 2018. 2021. Available online: https://doi.pangaea.de/10.1594/PANGAEA.926834 (accessed on 4 June 2024).
42. Gatti, L.V.; Correa, C.C.S.; Domingues, L.G.; Marani, L.; Meireles, F.; Crispim, S.P.; Neves, R.L.; Baggio, G.; Santana, R.; Costa, W.R.D. CO2 Vertical Profiles on Four Sites over Amazon from 2019 to 2020. 2023. Available online: https://doi.pangaea.de/10.1594/PANGAEA.949643 (accessed on 4 June 2024).
43. Kuze, A.; Suto, H.; Nakajima, M.; Hamazaki, T. Thermal and near infrared sensor for carbon observation Fourier-transform spectrometer on the Greenhouse Gases Observing Satellite for greenhouse gases monitoring. *Appl. Opt.* **2009**, *48*, 6716–6733. [CrossRef] [PubMed]
44. Yokota, T.; Yoshida, Y.; Eguchi, N.; Ota, Y.; Tanaka, T.; Watanabe, H.; Maksyutov, S. Global Concentrations of CO_2 and CH4 Retrieved from GOSAT: First Preliminary Results. *Sola* **2009**, *5*, 160–163. [CrossRef]
45. Someya, Y.; Yoshida, Y.; Ohyama, H.; Nomura, S.; Kamei, A.; Morino, I.; Mukai, H.; Matsunaga, T.; Laughner, J.L.; Velazco, V.A.; et al. Update on the GOSAT TANSO–FTS SWIR Level 2 retrieval algorithm. *Atmos. Meas. Tech.* **2023**, *16*, 1477–1501. [CrossRef]
46. Yoshida, Y.; Someya, Y.; Ohyama, H.; Morino, I.; Matsunaga, T.; Deutscher, N.M.; Griffith, D.W.T.; Hase, F.; Iraci, L.T.; Kivi, R.; et al. Quality evaluation of the column-averaged dry air mole fractions of carbon dioxide and methane observed by GOSAT and GOSAT-2. *SOLA* **2023**, *19*, 173–184. [CrossRef]
47. Connor, B.; Boesch, H.; Toon, G.; Sen, B.; Miller, C.; Crisp, D. Orbiting Carbon Observatory: Inverse method and prospective error analysis. *J. Geophys. Res.* **2008**, *113*, D05305. [CrossRef]
48. Tiwari, Y.K.; Guha, T.; Valsala, V.; Lopez, A.S.; Cuevas, C.; Fernandez, R.P.; Mahajan, A.S. Understanding atmospheric methane sub-seasonal variability over India. *Atmos. Environ.* **2020**, *223*, 117206. [CrossRef]
49. Zeng, J.; Nojiri, Y.; Landschützer, P.; Telszewski, M.; Nakaoka, S. A Global Surface Ocean fCO_2 Climatology Based on a Feed-Forward Neural Network. *J. Atmos. Ocean. Technol.* **2014**, *31*, 1838–1849. [CrossRef]
50. Zeng, J. Global Surface Ocean CO2 Concentration and Uptake Estimated Using a Neural Network, ver.2020.1. 2020. Available online: https://www.nies.go.jp/doi/10.17595/20201020.001-e.html (accessed on 7 May 2021).
51. Kaiser, J.W.; Heil, A.; Andreae, M.O.; Benedetti, A.; Chubarova, N.; Jones, L.; Morcrette, J.J.; Razinger, M.; Schultz, M.G.; Suttie, M.; et al. Biomass burning emissions estimated with a global fire assimilation system based on observed fire radiative power. *Biogeosciences* **2012**, *9*, 527–554. [CrossRef]
52. Zeng, J. A Data-Driven Upscale Product of Global Gross Primary Production, Net Ecosystem Exchange and Ecosystem Respiration. Ver. 2020.1. 2020. Available online: https://www.nies.go.jp/doi/10.17595/20200227.001-e.html (accessed on 9 March 2020).
53. Zeng, J.; Matsunaga, T.; Tan, Z.-H.; Saigusa, N.; Shirai, T.; Tang, Y.; Peng, S.; Fukuda, Y. Global terrestrial carbon fluxes of 1999–2019 estimated by upscaling eddy covariance data with a random forest. *Sci. Data* **2020**, *7*, 313. [CrossRef]
54. Oda, T.; Maksyutov, S.; Andres, R.J. The Open-source Data Inventory for Anthropogenic CO_2, version 2016 (ODIAC2016): A global monthly fossil fuel CO_2 gridded emissions data product for tracer transport simulations and surface flux inversions. *Earth Syst. Sci. Data* **2018**, *10*, 87–107. [CrossRef] [PubMed]
55. Basu, S.; Nassar, R. Fossil Fuel CO2 Emissions for the OCO2 Model Intercomparison Project (MIP). 2021. Available online: https://zenodo.org/records/4776925 (accessed on 28 June 2022).
56. Belikov, D.A.; Maksyutov, S.; Yaremchuk, A.; Ganshin, A.; Kaminski, T.; Blessing, S.; Sasakawa, M.; Gomez-Pelaez, A.J.; Starchenko, A. Adjoint of the global Eulerian-Lagrangian coupled atmospheric transport model (A-GELCA v1.0): Development and validation. *Geosci. Model Dev.* **2016**, *9*, 749–764. [CrossRef]

57. Nayagam, L.; Maksyutov, S.; Oda, T.; Janardanan, R.; Trisolino, P.; Zeng, J.; Kaiser, J.W.; Matsunaga, T. A top-down estimation of subnational CO_2 budget using a global high-resolution inverse model with data from regional surface networks. *Environ. Res. Lett.* **2023**, *19*, 014031. [CrossRef]
58. Ciais, P.; Yao, Y.; Gasser, T.; Baccini, A.; Wang, Y.; Lauerwald, R.; Peng, S.; Bastos, A.; Li, W.; Raymond, P.A.; et al. Empirical estimates of regional carbon budgets imply reduced global soil heterotrophic respiration. *Natl. Sci. Rev.* **2020**, *8*, nwaa145. [CrossRef] [PubMed]
59. Kondo, M.; Patra, P.K.; Sitch, S.; Friedlingstein, P.; Poulter, B.; Chevallier, F.; Ciais, P.; Canadell, J.G.; Bastos, A.; Lauerwald, R.; et al. State of the science in reconciling top-down and bottom-up approaches for terrestrial CO_2 budget. *Glob. Change Biol.* **2020**, *26*, 1068–1084. [CrossRef]
60. Deng, Z.; Ciais, P.; Hu, L.; Martinez, A.; Saunois, M.; Thompson, R.L.; Tibrewal, K.; Peters, W.; Byrne, B.; Grassi, G.; et al. Global Greenhouse Gas Reconciliation 2022. *Earth Syst. Sci. Data Discuss.* **2024**, *2024*, 1–47.
61. Regnier, P.; Friedlingstein, P.; Ciais, P.; Mackenzie, F.T.; Gruber, N.; Janssens, I.A.; Laruelle, G.G.; Lauerwald, R.; Luyssaert, S.; Andersson, A.J.; et al. Anthropogenic perturbation of the carbon fluxes from land to ocean. *Nat. Geosci.* **2013**, *6*, 597–607. [CrossRef]
62. Raju, A.; Sijikumar, S.; Burman, P.K.D.; Valsala, V.; Tiwari, Y.K.; Mukherjee, S.; Lohani, P.; Kumar, K. Very high-resolution Net Ecosystem Exchange over India using Vegetation Photosynthesis and Respiration Model (VPRM) simulations. *Ecol. Model.* **2023**, *481*, 110340. [CrossRef]
63. Nayak, R.K.; Mishra, N.; Dadhwal, V.K.; Patel, N.R.; Salim, M.; Rao, K.H.; SDutt, C.B. Assessing the consistency between AVHRR and MODIS NDVI datasets for estimating terrestrial net primary productivity over India. *J. Earth Syst. Sci.* **2016**, *125*, 1189–1204. [CrossRef]
64. Gahlot, S.; Shu, S.; Jain, A.K.; Baidya Roy, S. Estimating Trends and Variation of Net Biome Productivity in India for 1980–2012 Using a Land Surface Model. *Geophys. Res. Lett.* **2017**, *44*, 11,573–11,579. [CrossRef]
65. Canadell, J.G.; Monteiro, P.M.S.; Costa, M.H.; da Cunha, L.C.; Cox, P.M.; Eliseev, A.V.; Henson, S.; Ishii, M.; Jaccard, S.; Koven, C.; et al. Global Carbon and other Biogeochemical Cycles and Feedbacks. In *Climate Change 2021: The Physical Science Basis. Contribution of Working Group I to the Sixth Assessment Report of the Intergovernmental Panel on Climate Change*; Cambridge University Press: Cambridge, UK, 2021; pp. 673–816. [CrossRef]
66. Patra, P.K.; Canadell, J.G.; Houghton, R.A.; Piao, S.L.; Oh, N.H.; Ciais, P.; Manjunath, K.R.; Chhabra, A.; Wang, T.; Bhattacharya, T.; et al. The carbon budget of South Asia. *Biogeosciences* **2013**, *10*, 513–527. [CrossRef]
67. Rao, A.S.; Bala, G.; Ravindranath, N.H.; Nemani, R. Multi-model assessment of trends, variability and drivers of terrestrial carbon uptake in India. *J. Earth Syst. Sci.* **2019**, *128*, 99. [CrossRef]
68. Friedlingstein, P.; O'Sullivan, M.; Jones, M.W.; Andrew, R.M.; Gregor, L.; Hauck, J.; Le Quéré, C.; Luijkx, I.T.; Olsen, A.; Peters, G.P.; et al. Global Carbon Budget 2022. *Earth Syst. Sci. Data* **2022**, *14*, 4811–4900. [CrossRef]
69. Enting, I.G. *Inverse Problems in Atmospheric Constituent Transport*; Cambridge Atmospheric and Space Science Series; Cambridge University Press: Cambridge, UK, 2002; ISBN 978-0-521-81210-8.